



1 **Source apportionment of atmospheric mercury in the remote marine atmosphere: Mace**
2 **Head GAW station, Irish west coast**

3

4

5

Daniilo Custodio¹, Ralf Ebinghaus¹, T. Gerard Spain² and Johannes Bieser¹

6

7

¹ Helmholtz-Zentrum Geesthacht, Institute of Coastal Research, Max-Planck-Str. 1, D-21502 Geesthacht, Germany.

8

² National University of Ireland, Galway, Ireland.

9

10 Abstract

11 We examined recent atmospheric mercury concentrations measured with a high temporal resolution
12 of 15 min. at Mace Head, a GAW station on the west coast of Ireland. We attributed a direct
13 contribution of 34% (0.44 ng m⁻³) to primary sources. Additionally, a steep decline (0.05 ng year⁻¹) in
14 mercury concentrations was observed between 2013 and 2018.

15 Using a stereo algorithm we reconstructed 99.9% of the atmospheric mercury. A conservative
16 analysis demonstrated no decreasing of TGM associated with atmospheric species typically used as
17 tracers for oceanic emissions. The results show that the atmospheric mercury mass is mainly loaded in
18 a baseline factor with an on-going decline. Moreover, we exploit temporal variation and wind pattern
19 effects in the measured atmospheric species, the results show that the diurnal variation and
20 seasonality in TGM observed in Mace Head is closely related to other species linked to primary sources
21 and can be explained by transport from continental areas.

22

23

24 **1. Introduction**

25 Atmospheric mercury is a bioaccumulative, toxic pollutant with the potential to be transported over
26 large distances that poses a significant public health and environmental problem (WHO, 2007).

27 Despite efforts by governments and international agencies as well as the private sector to reduce
28 mercury release into the environment, current environmental levels are often still of concern.

29 Atmospheric mercury is emitted from both natural and anthropogenic sources as well as through
30 recycling of past emissions. Natural sources are comprised of release from volcanoes, weathering of
31 rocks, forest fires and oceanic emissions. Anthropogenic sources are related to fossil fuel combustion,
32 cement production, industrial activities, mining and municipal or medical waste incineration. Mercury
33 is also reintroduced into the atmosphere through natural processes such as oceanic evaporation after
34 reduction of inorganic oxidized Hg in anaerobic environments, which leads to global cycling of this
35 element (Corbitt et al., 2011; Streets et al., 2011). The source contribution, as well as the life-time of
36 atmospheric mercury, is only roughly estimated.

37 The 2018 Global Mercury Assessment (UN, 2018) reveals that primary anthropogenic mercury
38 emissions into the air are 2220 t/y, also indicating an increase of 20% from such sources in recent



39 years. The 2018 UNEP Report (AMAP/UNEP, 2018) presents an inventory for the year 2015, which
40 indicates that the greatest atmospheric mercury emissions resulted from combustion of fossils fuels,
41 mainly coal. While mercury in the atmosphere is chemically inert, once released into this environment,
42 all sources are of concern.

43 To compile a global assessment based on inventories requires a number of assumptions and
44 generalizations (AMAP/UNEP, 2018). Several discrepancies are observed in the mass balance-based
45 estimation: there can be large differences between estimates, and it is important to recognize that
46 there are sources of error in all methods for estimating mercury emissions.

47 Here we report concentrations of atmospheric mercury (TGM: total gaseous mercury) measured from
48 January 2013 to March 2018 at Mace Head. Mace Head station is located within the central North
49 Eastern Atlantic region and based on a GEOS-Chem simulation it is one of the most influenced
50 region by a decreasing mercury trend in ocean surface water, according to Soerensen et al.
51 (2012).

52 Using the relationship between mercury and other chemical atmospheric trace species (O_3 , CFC-12,
53 CCl_4 , N_2O , CH_4 , $CHCl_3$, CO and H_2) and meteorological data (wind speed and direction), we performed
54 a mass balance to reconstruct atmospheric mercury. Solved by positive matrix factorization, the total
55 mercury mass was distributed into four different factors, classified as baseline, combustion, oceanic
56 and a fourth factor and then each of them was assessed for source trends.

57 Time series analysis of atmospheric mercury concentrations at Mace Head were already
58 reported by Weigelt et al. (2015) and Ebinghaus et al. (2011).

59 In this work we apply a new approach for source apportionment and extend the time series
60 analysis up to March 2018.

61

62 **2. Experimental Setup**

63

64 **2.1. Sampling site and analytical methods**

65 Mace Head atmospheric research station is located on the west coast of Ireland at 53.33°N and 9.54°W,
66 55 km from Galway (80,000 inhabitants), the nearest city with significant industrial activity. It is a GAW
67 baseline station, exposed to the North Atlantic Ocean and is an ideal location to study both natural
68 and anthropogenic trace constituents in marine and continental air masses (Stanley et al., 2018).

69 In addition to atmospheric mercury, meteorological parameters are routinely monitored
70 (<https://www.met.ie/>). Atmospheric CFC-11, CFC-12, $CHCl_3$, CCl_4 , N_2O , CH_4 , CO and H_2 are measured
71 (Figure S1) as part of the AGAGE project (<https://agage.mit.edu/>).



72 TGM is monitored by an automated dual channel, single amalgamation, cold vapour atomic
73 fluorescence analyser (Tekran Analyzer Model 2537B, Tekran Inc., Toronto, Canada) described by
74 Ebinghaus et al. (2011).

75 The air-sampling inlet is located on a tower at 10m agl (18m amsl). Air is sampled at a flowrate of 1
76 L/min through unheated PTFE tubing (1/4" O.D.) to the instrument, which is located in an air-
77 conditioned laboratory. As reported by Weigelt (2015), a PTFE pre-filter (pore size 0.2 mm) at the inlet
78 of the instrument protects the sampling cartridges from contamination by particles. The device is
79 operated with a temporal resolution of 15 minutes, calibrated every 25 hours using an internal mercury
80 permeation source. The device has a detection limit of $\sim 0.1 \text{ ng m}^{-3}$ (Weigelt et al., 2015).

81 Furthermore, wind streamlines for near surface level conditions were assessed from
82 <https://earth.nullschool.net/> and long-range transport of air pollutants was calculated using the
83 HYSPLIT model (Draxler and Rolph, 2003) from NOAA (National Oceanic and Atmospheric
84 Administration).

85

86 2.2. Source assessment / Probability mass function

87 Apportionment of atmospheric species is often performed by receptor models that are based on the
88 mass conservation principle:

89 The inclusion of the potential rotated infinity matrices transformation produces factors that
90 appear to be closer to realistic chemical profiles of sources:

$$91 \quad x_{ij} = \sum_{k=1}^p g_{ik} f_{jk} \quad i=1,2,\dots,m \quad j=1, 2,\dots, n \quad (1)$$

92 where x_{ij} is the concentration of the species j in the i^{th} sample, g_{ik} is the contribution of the factor
93 (associated to a source) k^{th} in the i^{th} sample and f_{jk} is the concentration of the species j in factor k as
94 presented by Paatero and Hopke (2003) and described by Comero et al. (2009). This equation can be
95 solved by the probability mass function in *positive matrix factorization* (PMF) (Paatero and Tapper,
96 1994) with the Multilinear Engine (ME-2) developed by Paatero (1999) and implemented in Version 5
97 of the US EPA PMF (<https://www.epa.gov/air-research/positive-matrix-factorization-model-environmental-data-analyses>).

99 In this study, PMF was applied to the Mace Head dataset with an hourly time resolution for the period
100 2013 to 2018. The results were constrained to provide positive factor contribution. The uncertainty
101 input in the matrix was estimated based on the analytical accuracy of each individual species.

102 PMF is a stereo algorithm where analytical data sets are combined to create fingerprints and the profile
103 is used to assess the contribution of each source based on the mass load, also providing a robust
104 uncertainty estimation and source diagnostics. The method provides a better solutions and time
105 resolution of sources than principal component analysis (PCA) (Huang et al., 1999) or chemical mass



106 balance (CMB) since PMF can generate source profiles (“learning algorithm”) and let input of
107 uncertainties which allow individual treatment of matrix elements.

108 In the PMF the weighted factorization regression analysis is based on positive rotatable factorization of
109 non-singular matrix T ;

$$110 X = F G + E = G T T^{-1} F + E = \overline{G} \overline{F} + E, \quad (2)$$

111 where the new rotated factors are

112 $\overline{G} = G T$ and $\overline{F} = T^{-1} F$ as reported by Comore et al. (2009), then the factors are non-negatively
113 constrained.

114 Factors contributions are chosen on the basis of a matching strength score by using a form of discrete
115 correlation. At the first interaction any matches which have the highest matching strength for
116 primitives mass reconstruction that formed them are immediately chosen as reconstructed. Then, in
117 accordance with the uniqueness constraint, all other matches associated with the primitives that have
118 been formed for each chosen match are eliminated from further consideration. This allows further
119 matches that were not either previously accepted or eliminated to propagate the process of PMF to a
120 satisfactory solution if the propagation converges.

121

122 3. Results

123 Time series of TGM concentrations composed of 48,914 hours of measurements covering the period
124 from January 2013 to March 2018 are given in Figure 1. Concentrations range from 0.9 to 3.3 ng m⁻³,
125 displaying a central tendency of 1.3 ± 0.2 ng m⁻³. TGM concentrations in the northern hemisphere have
126 been decreasing in recent decades (Ebinghaus et al., 2011; Slemr et al., 2003). For instance, Ebinghaus
127 et al. (2011) reported a decline trend of 0.028 ± 0.01 ng m⁻³ yr⁻¹ between 1996 to 2009. Account the
128 more recent years (1996 to 2018), this decline continued with approximately 0.025 ± 0.04 ng m⁻³ yr⁻¹,
129 figure 2. This observation could reflect a trend in global emissions, as mercury, roughly, has an
130 atmospheric lifetime of 0.5 to 1 year (Holmes et al., 2006; Lindberg et al., 2007; Si and Ariya 2018). The
131 increasing improvement of manufacturing processes involving mercury and regulations limiting the
132 emissions from coal-fired power plants since the 1980s (Hylander and Meili, 2003; Pirrone et al., 2009)
133 could be a possible reason for this observed decline at Mace Head. Jiskra et al. (2018) report the Hg⁰
134 uptake by vegetation as an alternative mechanism for driving mercury depletion in the Northern
135 Hemisphere atmosphere over the past 20 years.

136 However, this decreasing trend is inconsistent with the increased emissions from 1990 to 2015, as
137 indicated by anthropogenic Hg emission inventories (e.g., UN, 2018 and AMAP/UNEP, 2018).

138 3.1. Temporal and wind pattern effects in mercury concentrations



139 Plots of TGM as a function of wind speed and direction can be seen in Figure 3 as well as the polar
140 frequency plot of wind direction. Concentrations of mercury are higher when winds come from the
141 east (continental air masses) and lower for winds from the west and northwest (Atlantic air masses).
142 The higher concentrations to the east are likely to be influenced by urban agglomerations, such as in
143 Galway, Dublin or even the UK and continental Europe. These higher levels observed to the east are
144 associated with relatively strong wind speeds of 15ms^{-1} , which could indicate a relatively distant
145 source. Furthermore, an increase of TGM with strong winds of 20ms^{-1} was observed, indicating sources
146 at further distances in air masses coming from westerly and south-westerly directions. 96-hour back
147 trajectories show that these high TGM concentrations at Mace Head were affected by air mass
148 transport from the Iberian Peninsula and long-range transport from North America.

149 Higher mercury concentrations under the influence of easterly and strong westerly/south-
150 westerly winds closely resemble those of other pollutants that are also closely linked to
151 anthropogenic emissions, such as carbon monoxide, and suggest TGM enrichment from
152 continental air masses.

153 The polar plot shows low concentrations of mercury associated with strong and weak winds
154 coming from the North Sea and nearby land air masses, with $\text{in} < 10\text{m s}^{-1}$.

155 The diurnal cycle of elemental mercury (Hg^0) has been discussed extensively (Laurier et al., 2003;
156 Weiss-Penzias et al., 2003; Laurier and Mason, 2007; Xia et al., 2010; Obrist et al., 2011; Moore et al.,
157 2013; Wang et al., 2014; Ci et al., 2015; Wang et al., 2017; Castagna et al., 2018, Jiskra et al., 2018).
158 Kalinchuk et al. (2019) reported solar radiation-driven increase and decrease of mercury
159 concentrations in the Sea of Japan and in the Sea of Okhotsk, respectively. They assumed that the
160 decrease in Hg^0 concentrations in the marine boundary layer during daytime is mainly caused by its
161 oxidation, catalyzed by active halogen species (mainly by atomic bromine radicals), which are released
162 from sea salt aerosols as Br_2 and could be transformed into reactive forms as a result of photolysis
163 (Holmes et al., 2009; Sprovieri et al., 2010; Mao and Talbot, 2012; Moore et al., 2013; Si and Ariya,
164 2018). However, the absence of a diurnal cycle for mercury is reported in several studies and more
165 research should be done to confirm the catalytic photolysis oxidation, as large uncertainties exist in
166 the gas-phase reaction of mercury (Si and Ariya, 2018).

167 With a standard electrode potential (E^0) of $+0.85\text{V}$ and a kinetic coefficient of reactivity of $<9.8 \times 10^{-13}$
168 to $2.1 \times 10^{-12}\text{cm}^3\text{molec}^{-1}\text{s}^{-1}$, at 1 atm and 298 K (Khalizov et al., 2003; Shepler et al., 2007; Subir at
169 al., 2011; Sun et al., 2016), Hg^0 is quite a stable vapour gas, and a significant daily mass depletion by
170 photooxidation is very unlikely.

171 Seasonality and diurnal patterns for mercury concentrations at Mace Head have been detected, but
172 similar patterns were observed for CO. As presented in Figure 4, wind direction was a driving factor for
173 diurnal cycling of TGM at Mace Head as well as for CO and CHCl_3 . Winds from the east (land breezes)



174 showed sharp increases of TGM, CO, CFC-12 and CCl₄ (figure 3 and Figure S3). Conversely, an increase
175 of CHCl₃ in offshore winds (sea breezes) was observed.

176 Mace Head is mostly influenced by air masses from the Atlantic Ocean, however, as a coastal site can
177 be affected by on-shore breezes blowing from land to the North Atlantic. Daily fluctuations of wind
178 speed and direction in coastal areas are a result of differences in air pressure created by the different
179 heat capacities of water and dry land (Yan Y.Y., 2005).

180 Decrease of atmospheric mercury concentrations during warm periods has often been linked to
181 increased Hg²⁺ by catalytic mercury oxidation in the surface layer of the sea due to several chemical
182 and biological processes, mainly controlled by solar radiation (Kalinchuk et al., 2019 and references
183 therein). Si and Ariya (2018) and references therein reported maximum oxidation of mercury in
184 summer based on several atmospheric models but failed to reconstruct observed summer depletion
185 of atmospheric mercury at monitoring sites in North America and Europe. Furthermore, deposition
186 models could not predict the observed large seasonal variability of either Hg oxidation or wet
187 deposition flux (Travnikov et al., 2017).

188 Figure 4 shows that the decrease of TGM during summer is closely related to CO depletion in this
189 season.

190 In addition, it was observed similarity among TGM depletion during summer, enhancement during
191 autumn and seasonality of chloroform (CHCl₃). Decreased emissions of CHCl₃ from seawater or more
192 intense depletion by photooxidation during summer may be possible explanations. It should be noted
193 that any photochemical pattern of those species must be considered with caution because CHCl₃ is a
194 short-lived species (lifetime ~0.5yr), mainly produced in the ocean by biological processes that follow
195 a different oxidation pathway than mercury (Khalil and Rasmussen, 1999). It should also be noted that
196 wind pattern differences were observed within one year for Mace Head: strong winds during winter
197 predominately comes from the sea, and relatively calm winds during summer (Figure S2). This should
198 also be reflected in the observed seasonality of TGM concentrations.

199 The results obtained during this study show that the seasonality in TGM observed in Mace Head is
200 closely related to other species linked to primary sources and can be explained by transport from
201 continental areas.

202

203 3.2. Source apportionment

204 Figure 1 shows the set of four factors reconstructing atmospheric mercury concentrations obtained
205 from the PMF solution. As reported by Henry (1991), the first set of natural physical constraints of the
206 system to be considered in any approach for identifying and quantifying source mass contributions
207 must be the reconstruction of the original data set by the algorithm—that is, the solution must explain
208 the observations. Figure 5 shows that the sum of the predicted elemental mass contributions for all



209 sources is almost the same as the total TGM measured. Lower reconstruction performance was
210 observed in particular for concentrations higher than 2 ng m^{-3} , which make up 0.44% of the
211 observations.

212 The first factor with a loading of 66% of TGM mass (0.88 ng m^{-3}) was labelled as baseline because it
213 does not show any wind pattern, carries high loads of long-lived species such as CFCs and low loads of
214 CO or sea-borne trace gas species. The PMF results show a statistically significant decrease in the
215 baseline factor that could explain almost all of the trend changes in atmospheric mercury. This suggests
216 a major decrease of anthropogenic inputs on a global scale. Slemr et al. (2011) reported a worldwide
217 trend of atmospheric mercury, showing an equally strong decrease in the northern and southern
218 hemispheres, which supports the argument of baseline-driven TGM decline.

219 According to Streets et al. (2011), anthropogenic Hg emissions in the USA and Europe decreased by
220 20% and 40%, respectively, from 1990 to 2008. However, emissions on a global scale, particularly from
221 East Asia, are poorly reported (UN, 2018), even for most of the countries that are signatories of
222 Minamata convention (UN, 2019). Moreover, the total emissions from small scale artisanal gold mining
223 are highly uncertain estimates.

224 Another possible explanation for the declining trend may be the Hg^0 atmospheric life-cycling reduction
225 due to atmospheric acidification caused by CO_2 potential (E°) to force elemental mercury oxidation.

226 As reported by Slemr et al. (2011) and references therein, increase in the atmospheric reactivity can
227 induce large decreasing trends in the concentration of many long-lived substances. Clerbaux and
228 Cunnold, (2007) did not observe lifetime changes for halogenated and other greenhouse gases,
229 however, changes in oxidation rates of elemental mercury in the atmosphere could follow different
230 kinetics. Furthermore, the increasing UV radiation and the shifting solar radiation to shorter
231 wavelengths could also intensify the oxidation of elemental mercury into Hg^{2+} (IPCC, 2007; Qureshi et
232 al., 2010). Jiskra et al. (2018), on the other hand, hypothesize that increased vegetation uptake could
233 be a reason for decreasing atmospheric mercury concentrations in recent years.

234 A second factor that contributes to mercury with $0.27 \pm 0.13 \text{ ng m}^{-3}$ (21 %) and is characterised by a
235 high load of CO and labelled as combustion. A decreasing trend was observed in this factor, but this is
236 a more complex case because a higher load of Hg in the combustion factor could be strongly influenced
237 by wind direction, as shown in Figure 6. For the potential seasonality, significant trends are also difficult
238 to establish due to the relatively short time series. The Global Mercury Assessment inventory (UN,
239 2018) estimates the contribution of combustion sources to atmospheric mercury at 24%.

240 The wind patterns for the baseline, combustion and sea factors (discussed below) as displayed in the
241 polar plot of Figure 6 indicate an interpretation of the PMF profile with “combustion” being mostly
242 associated with easterly transport, “sea” being linked to north-westerly and south-westerly winds. The
243 “baseline” factor does not correlate with any significant wind patterns.



244 The seasonality observed in the factors fingerprinted by CHCl_3 and CO (Figure 7) should, however, be
245 considered with caution because those short-lived species (CHCl_3 4-5 months and CO 1-3 months) have
246 lifetimes that vary by season, which can dampen mercury load into its factor during summer. However,
247 no seasonality was observed for the baseline factor, linking lower concentrations of mercury in the
248 warm season mainly to transport or evasion patterns and less to deposition by oxidation.

249 Human activity has substantially increased the ocean mercury reservoirs and consequently the fluxes
250 between the ocean and atmosphere (Strode et al., 2007; Smith-Downey et al., 2010).

251 The residence time of mercury in the ocean is substantially longer than in the atmosphere, ranging
252 from years to decades or millennia (Strode et al., 2007; Primeau and Holzer, 2006). Acidification of
253 oceans, climate change, excess nutrient inputs, and pollution are fundamentally changing the ocean's
254 biogeochemistry (Doney, 2010) and will certainly also influence mercury ocean-air fluxes (Slemr et al.,
255 2011). The extent, however, and even the direction of the change is unknown.

256 Mason et al. (2012) estimate that global oceanic Hg^0 evasion to be comparable to anthropogenic
257 emissions, and Sunderland and Mason (2007) attributed the mercury emitted from seawater in the
258 North Atlantic to the legacy of 20th-century anthropogenic sources in Europe and North America.

259

260 This study shows an oceanic contribution of 13% ($0.17 \pm 0.07 \text{ ng m}^{-3}$) to atmospheric TGM at Mace
261 Head station. Based on atmospheric mercury concentration trends in the subsurface seawater
262 Soerensen et al. (2012) predicted a decrease of approximately $0.045 \text{ ng m}^{-3} \text{ yr}^{-1}$ of oceanic mercury
263 emissions into the air over the North Atlantic. They also argued, based on cruise data, that the decrease
264 of oceanic emissions is forcing the atmospheric trend. In this study, based on the PMF solution, we
265 found no evidence for a decreasing mercury load in the oceanic factor, which could be traced by CHCl_3
266 and CH_4 concentrations.

267 A fourth factor with a high load of O_3 and CO was found by the PMF solution which appeared to be
268 irrelevant for the mercury mass balance, as its load was just 0.003 ng m^{-3} . However, for atmospheric
269 mercury concentrations higher than 2 ng m^{-3} this factor had a load of 0.57 ng m^{-3} . In addition, with 0.53
270 ng m^{-3} the mercury load in the combustion factor for concentrations higher than 2 ng m^{-3} is twice as
271 high as for concentrations below 2 ng m^{-3} in this sector. (Figure 8).

272 Moreover, we find from the PMF solution that the decrease of atmospheric mercury is linked less to
273 oceanic emissions and is explained mainly by a baseline factor with a low load of short-lived species
274 with significant anthropogenic sources, such as CO and O_3 , as well as a low load of sea trace species,
275 such as CHCl_3 and CH_4 .

276 On the other hand, a decrease in mercury is observed in the factor with high loading of long-lived
277 species such as CFCs. However, the presented solution for apportionment of atmospheric mercury has
278 restrictions and requires further consideration, as the mercury sources are complex and numerous,
279 and merely a few source tracers were used in this study.



280
281
282
283
284

4. Conclusions

285 This study presents a comprehensive source assessment of atmospheric mercury measured
286 at Mace Head, a baseline station with a long-term decreasing trend of TGM. Positive matrix
287 factorization was applied to a set of atmospheric mercury data from 2013 to 2018 with high
288 temporal resolution. The profiles of source factor contributions indicate that baseline (0.86 ng
289 m⁻³, 66%) and combustion processes (0.27 ng m⁻³, 21%) are the controlling factors of mercury
290 in the atmosphere at this remote coastal measurement location. The high load of mercury in
291 the baseline factor reflects the relatively long lifetime of this species in the atmosphere.

292 Biogenic activities in the ocean were identified as another primary source, contributing 13 %
293 (0.17 ng m⁻³).

294 Therefore, based on the analysis of temporal changes in the sources, no decreasing in the
295 oceanic factor in the period of this study could be detected. The decrease in atmospheric
296 mercury concentrations was linked to the baseline factor. Source contributions by wind sector
297 were also exploited, based on directional wind dependence of source loadings from the PMF
298 analysis. The patterns are also consistent with the location of the sources: oceanic sources
299 coming from the west (Atlantic) and anthropogenic sources coming from east (Europe) of
300 Mace Head. Furthermore, more extensive and detailed descriptions concerning mercury
301 sources is needed to confirm and evaluate the reported trends, which then can have great
302 relevance for policy and regulations in light of the Minamata convention.

303

304 Acknowledgments

305 Acknowledgements. This work was funded by the iGOSP ERA-PLANET and E-SHAPE
306 “EUROGEOSS” Showcase projects. The author acknowledges the Mace Head
307 Observatory for all data provision. The authors gratefully acknowledge the NOAA
308 Air Resources Laboratory (ARL) for the provision of the HYSPLIT transport and
309 dispersion model and READY website (<http://www.ready.noaa.gov>).
310

311

312 References

313

314 AMAP/UNEP: Technical Background Report for the Global Mercury Assessment 2018. United Nations
315 Environment Programme (UNEP), 2018.
316 Castagna, J., Bencardino, M., D'Amore, F., Esposito, G., Pirrone, N., Sprovieri, F.: Atmospheric mercury species
317 measurements across the Western Mediterranean region: Behaviour and variability during a 2015 research
318 cruise campaign. Atmos. Environ. 173, 108e126. <https://doi.org/10.1016/J.ATMOENV.2017.10.045>, 2018.



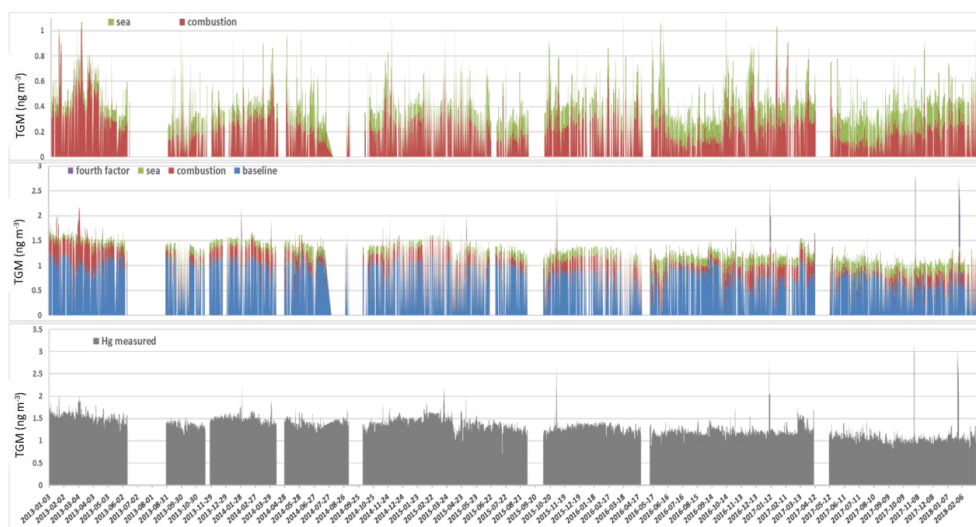
- 319 Ci, Z., Wang, C., Wang, Z., Zhang, X.: Elemental mercury (Hg⁰) in air and surface waters of the Yellow Sea during
320 late spring and late fall 2012: Concentration, spatial-temporal distribution and air/sea flux. *Chemosphere* 119,
321 199e208. <https://doi.org/10.1016/j.chemosphere.2014.05.064>, 2015.
- 322 Clerbaux, C., and Cunnold, D.M.: Long-lived compounds, in: “Scientific Assessment of Ozone Depletion: 2006”,
323 WMO, Geneva, 2007.
- 324 Comero, S., Capitani, L., Gawlik, B.M.: Positive Matrix Factorisation (PMF): An introduction to the chemometric
325 evaluation of environmental monitoring data using PMF. European Commission. EUR 23946 EN, ISBN 978-92-
326 79-12954-4 ISSN 1018-5593, DOI 10.2788/2497, 2009.
- 327 Corbitt, E. S., D. J. Jacob, C. D. Holmes, D. G. Streets, and E. M. Sunderland: Global source receptor relationships
328 for mercury deposition under present-day and 2050 emissions scenarios, *Environ. Sci. Technol.*, 45, 10,477–
329 10,484, doi:10.1021/es202496y, 2011.
- 330 Doney, S. C.: The growing human footprint on coastal and openocean biogeochemistry, *Science*, 328, 1512–
331 1516, 2010.
- 332 Draxler, R. R., and G. D. Rolph: HYSPLIT (HYbrid Single-ParticleLagrangian Integrated Trajectory) Model access via
333 NOAA ARLREADY Website, NOAA Air Resour. Lab., Silver Spring, Md. (Availableat
334 <http://www.arl.noaa.gov/ready/hysplit4.html>), 2003.
- 335 Ebinghaus, R., Jennings, S.G., Kock, H.H., Derwent, R.G., Manning, A.J., Spain, T.G.: Decreasing trend in total
336 gaseous mercury observations in baseline air at Mace Head, Ireland, from 1996 to 2009. *Atmos. Environ.* 45,
337 3475e3480, 2011.
- 338 Henry, R.C.: Multivariate Receptor Models, In: *Receptor Modeling for Air Quality Management*, P.K. Hopke, ed.,
339 Elsevier Science Publishers, Amsterdam, 117-147, 1991.
- 340 Holmes, C. D, Jacob, D. J. Yang, X.: Global lifetime of elemental mercury against oxidation by atomic bromine in
341 the free troposphere, *Geophys. Res. Lett.*, 33, L20808, doi:10.1029/2006GL027176, 2006.
- 342 Holmes, C.D., Jacob, D.J., Mason, R.P., Jaffe, D.A.: Sources and deposition of reactive gaseous mercury in the
343 marine atmosphere. *Atmos. Environ.* 43, 2278e2285. <https://doi.org/10.1016/J.ATMOSENV.2009.01.051>,
344 2009.
- 345 Huang, S., Rahn, K.A. Arimoto, R.: Testing and Optimizing Two Facot-Analysis Techniques on Aerosol at
346 Narragansett, Rhode Island, *Atmospheric Environ.* 33:2169-2185, 1999.
- 347 IPCC: *Climate Change 2007: Synthesis Report*, Geneva, Switzerland, 2007.
- 348 Hylander, L. D. Meili, M.: 500 years of mercury production: global annual inventory by region until 2000 and
349 associated emissions, *Sci. Total Environ.* 304, 13–27, 2003.
- 350 Kalinchuk, V., Aksentov, K., Karnaukh, V.: Gaseous elemental mercury (Hg(0)) in the surface air over the Sea of
351 Japan, the Sea of Okhotsk and the Kuril-Kamchatka sector of the Pacific Ocean in August-September 2017.
352 *Chemosphere* 224, 668e679, 2019.
- 353 Khalil, M.A.K., Rasmussen, R.A.: Atmospheric chloroform. 7, 1151-1158, 1999.
- 354 Khalizov, A.F., Viswanathan, B., Larregaray, P., Ariya, P.A.: Theoretical Study on the Reactions of Hg with
355 Halogens: Atmospheric Implications. *J. Phys. Chem. A*, 107, 6360–6365, 2003.
- 356 Jiskra, M., Sonke, J.E., Obrist, D., Bieser, J., Ebinghaus, R., Myhre, C.L., Pfaffhuber, K.A., Wängberg, I., Kyllönen,
357 K., Worthy, D., Martin, L.G., Labuschagne, C., Mkololo, T., Ramonet, M., Magand O., Dommergue. A.: A
358 vegetation control on seasonal variations in global atmospheric mercury concentrations. *NATURE*
359 *GEOSCIENCE | VOL 11 | APRIL 2018 | 244–250*, 2018.
- 360 Laurier, F., Mason, R.: Mercury concentration and speciation in the coastal and open ocean boundary layer. *J.*
361 *Geophys. Res.* 112, D06302. <https://doi.org/10.1029/2006JD007320>, 2007.
- 362 Laurier, F.J.G., Mason, R.P., Whalin, L.: Reactive gaseous mercury formation in the North Pacific Ocean's marine
363 boundary layer: A potential role of halogen, 2003.
- 364 Lindberg, S., Bullock, R., Ebinghaus, R., Engstrom, D., Feng, X., Fitzgerald, W., Pirrone, N., Prestbo, E., and
365 Seigneur, Ch.: A synthesis of progress and uncertainties in attributing the sources of mercury in deposition,
366 *Ambio* 36, 19–32, 2007.
- 367 Mao, H., Talbot, R.: Speciated mercury at marine, coastal, and inland sites in New England-Part 1: Temporal
368 variability. *Atmos. Chem. Phys.* 12, 5099e5112. <https://doi.org/10.5194/acp-12-5099-2012>, 2012.



- 369 Mason, R. P., Choi, A.L., Fitzgerald, W.F., Hammerschmidt, C.R., Lamborg, C.H., Soerensen, A.L., Sunderland, E.
370 M.: Mercury bio-geochemical cycling in the ocean and policy implication, *Environ. Res.*,
371 doi:10.1016/j.envres.2012.03.013, in press, 2012.
- 372 Moore, C.W., Obrist, D., Luria, M.: Atmospheric mercury depletion events at the Dead Sea: Spatial and temporal
373 aspects. *Atmos. Environ.* 69, 231e239. <https://doi.org/10.1016/J.ATMOSENV.2012.12.020>, 2013.
- 374 Obrist, D., Tas, E., Peleg, M., Matveev, V., Faïn, X., Asaf, D., Luria, M.: Bromine-induced oxidation of mercury in
375 the mid-latitude atmosphere. *Nat. Geosci.* 4, 22e26. <https://doi.org/10.1038/ngeo1018>, 2011.
- 376 Paatero, P.: The multilinear engine – a table-driven least squares program for solving multilinear problems,
377 including the n-way parallel factor analysis model, *J. Comput. Graph. Stat.*, 8, 854–888, 1999.
- 378 Paatero, P. and Hopke, P. K.: Discarding or downweighting high noise variables in factor analytic models, *Anal.*
379 *Chim. Acta*, 490, 277–289, 2003.
- 380 Paatero, P. and Tapper, U.: Positive matrix factorization: A non-negative factor model with optimal utilization of
381 error estimates of data values, *Environmetrics*, 5, 111–126, 1994.
- 382 Pirrone, N., Cinnirella, S., Feng, X., Finkelman, R. B., Friedli, H. R., Leaner, J., Mason, R., Mukherjee, A. B., Stracher,
383 G., Streets, D. G., and Telmer, K.: Global mercury emissions to the atmosphere from natural and
384 anthropogenic sources, in: *Mercury Fate and Transport in the Global Atmosphere*, edited by: Pirrone, N.,
385 Mason, R., 3–49, Springer, Dordrecht, 2009.
- 386 Primeau, F. W. and Holzer, M.: The ocean’s memory of the atmosphere: Residence-time and ventilation-rate
387 distributions of water masses, *J. Phys. Oceanography* 36, 1439–1456, 2006.
- 388 Qureshi, A., O’Driscoll, N. J., MacLeod, M., Neuhold, Y.-M., and Hungerbühler, K.: Photoreactions of mercury in
389 surface ocean water: Gross reaction kinetics and possible pathways, *Environ. Sci. Technol.* 44, 644–649, 2010.
- 390 Smith-Downey, N. V., Sunderland, E. M., and Jacob, D. J.: Anthropogenic impacts on global storage and emissions
391 of mercury from terrestrial soils: Insights from a new global model, *J. Geophys. Res.*, 115, G03008,
392 doi:10.1029/2009JG001124, 2010.
- 393 Shepler, B.C.; Balabanov, N.B.; Peterson, K.A.: Hg+Br→HgBr recombination and collision induced dissociation
394 dynamics. *J. Chem. Phys.*, 127, 164–304, 2007.
- 395 Si, L., Ariya, P.A.: Recent Advances in Atmospheric Chemistry of Mercury. *Atmosphere (Basel)* 9, 76.
396 <https://doi.org/10.3390/atmos9020076>, 2018.
- 397 Slemr, F., Brunke, E.G., Ebinghaus, R., and Kuss, J.: Worldwide trend of atmospheric mercury since 1995, *Atmos.*
398 *Chem. Phys.*, 11, 4779 – 4787, doi:10.5194/acp-11-4779-2011, 2011.
- 399 Slemr, F., Brunke, E.-G., Ebinghaus, R., Temme, C., Munthe, J., W€angberg, I., Schroeder, W., Steffen, A., Berg, T.:
400 Worldwide trend of atmospheric mercury since 1977. *Geophys. Res. Lett.* 30 (10), 1516.
401 <http://dx.doi.org/10.1029/2003GL016954>, 2003.
- 402 Soerensen, A.L., Jacob, D.J., Streets, D.G., Witt, M.L.I., Ebinghaus, R., Mason, R.P., Andersson, M., Sunderland,
403 E.M.: Multi-decadal decline of mercury in the North Atlantic atmosphere explained by changing subsurface
404 seawater concentrations. *Geophys. Res. Lett.* 39, L21810. <http://dx.doi.org/10.1029/2012GL053736>, 2012.
- 405 Sprovieri, F., Hedgecock, I.M., Pirrone, N.: An investigation of the origins of reactive gaseous mercury in the
406 Mediterranean marine boundary layer. *Atmos. Chem. Phys.* 10, 3985e3997. [https://doi.org/10.5194/acp-10-](https://doi.org/10.5194/acp-10-3985-2010)
407 [3985-2010](https://doi.org/10.5194/acp-10-3985-2010), 2010.
- 408 Stanley, K.M., Grant, A., O’Doherty, S., Young, D., Manning, A.L., Stavert, A.R., Gerard Spain, T.G., Salameh, P.K.,
409 Harth, C.M., Simmonds, P.G., Sturges, W.T., Oram, D.E. and Derwent, R.G.: Greenhouse gas measurements
410 from a UK network of tall towers: technical description and first results. *Atmos. Meas. Tech.*, 11, 1437–1458,
411 <https://doi.org/10.5194/amt-11-1437-2018>, 2018.
- 412 Subir, M.; Ariya, P.A.; Dastoor, A.P.: A review of uncertainties in atmospheric modeling of mercury chemistry I.
413 Uncertainties in existing kinetic parameters—Fundamental limitations and the importance of heterogeneous
414 chemistry. *Atmos. Environ.*, 45, 5664–5676, 2011.
- 415 Sun, G.; Sommar, J.; Feng, X.; Lin, C.-J.; Ge, M.; Wang, W.; Yin, R.; Fu, X.; Shang, L.: Mass-dependent and -
416 independent fractionation of mercury isotope during gas-phase oxidation of elemental mercury vapor by
417 atomic Cl and Br. *Environ. Sci. Technol.*, 50, 9232–9241, 2016.
- 418 Sunderland, E. M., and Mason, R.P.: Human impacts on open ocean mercury concentrations, *Global Biogeochem.*
419 *Cycles*, 21, GB4022, doi:10.1029/2006GB002876, 2007.

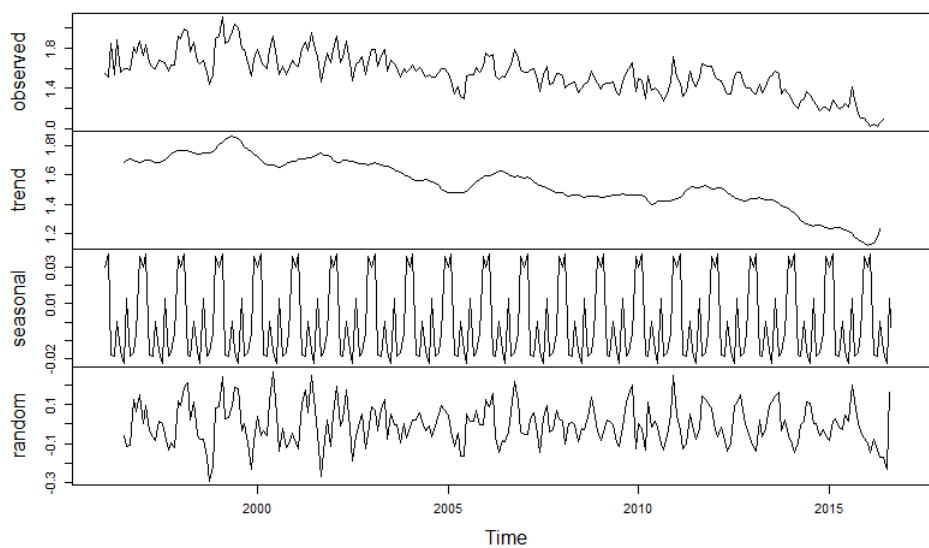


- 420 Streets, D. G., M. K. Devane, Z. Lu, T. C. Bond, Sunderland, E.M., and Jacob, D.J.: All-time releases of mercury to
421 the atmosphere from human activities, *Environ. Sci. Technol.*, 45 (24), 10,485–10,491,
422 doi:10.1021/es202765m, 2011.
- 423 Travníkov, O., Angot, H., Artaxo, P., Bencardino, M., Bieser, J., D'Amore, F., Dastoor, A., Simone, F.D., Diéguez,
424 M.d.C., Dommergue, A., et al.: Multi-model study of mercury dispersion in the atmosphere: Atmospheric
425 processes and model evaluation. *Atmos. Chem. Phys.*, 17, 5271–5295, 2017.
- 426 Strode, S. A., Jaegl'e, L., Selin, N. E., Jacob, D. J., Park, R. J., Yantoska, R. M., Mason, R. P., and Slemr, F.: Air-sea
427 exchange in the global mercury cycle, *Global Biogeochem. Cycles* 21, GB1017, doi:10.1029/2006GB002766,
428 2007.
- 429 UN, Global Mercury Assessment: Environment Programme. Chemicals and Health Branch Geneva_ Switzerland,
430 ISBN: 978-92-807-3744-8, 2018.
- 431 UN, Minamata Convention on Mercury: United Nation Environmental Program.
432 <http://www.mercuryconvention.org/Countries/Parties/tabid/3428/language/en-US/Default.aspx>, 2019.
- 433 Wang, Y., Liu, R., Li, Y., Cui, X., Zhou, J., Liu, S., Zhang, Y.: GEM in the marine atmosphere and air-sea exchange of
434 Hg during late autumn and winter cruise campaigns over the marginal seas of China. *Atmos. Res.* 191, 84e93.
435 <https://doi.org/10.1016/j.atmosres.2017.03.004>, 2017.
- 436 Wang, F., Saiz-Lopez, A., Mahajan, A.S., Gomez Martín, J.C., Armstrong, D., Lemes, M., Hay, T., Prados-Roman,
437 C.: Enhanced production of oxidised mercury over the tropical Pacific Ocean: a key missing oxidation pathway.
438 *Atmos. Chem. Phys.* 14, 1323e1335. <https://doi.org/10.5194/acp-14-1323-2014>, 2014.
- 439 Weiss Penzias, P., Jaffe, D.A., McClintick, A., Prestbo, E.M., Landis, M.S.: Gaseous Elemental Mercury in the
440 Marine Boundary Layer: Evidence for Rapid Removal in Anthropogenic Pollution, pp. 375e3763.
441 <https://doi.org/10.1021/es0341081>, 2003.
- 442 Weigelt, A., Ebinghaus, R., Manning, A.J., Derwent, R.G., Simmonds, P., Spain, T.G., Jennings, S.G., Slemr, F.:
443 Analysis and interpretation of 18 years of mercury observations since 1996 at Mace Head, Ireland.
444 *Atmospheric Environment* 100, 85 e 93, 2015.
- 445 Wilson, S., Munthe, J., Sundseth, K., Kindbom, K., Maxson, P., Pacyna, P., Steenhuisen, F.: Updating historical
446 global inventories of anthropogenic mercury emissions to air, AMAP Tech. Rep. 3, 14 pp., Arct. Monit. and
447 Assess. Programme, Oslo, 2010.
- 448 WHO -World Health Organization: EXPOSURE TO MERCURY: A MAJOR PUBLIC HEALTH CONCERN. 20 Avenue
449 Appia, CH-1211 Geneva-27, Switzerland (Document available online), 2007.
- 450 Xia, C., Xie, Z., Sun, L.: Atmospheric mercury in the marine boundary layer along a cruise path from Shanghai,
451 China to Prydz Bay, Antarctica. *Atmos. Environ.* 44, 1815e1821.
452 <https://doi.org/10.1016/J.ATMOSENV.2009.12.039>, 2010.
- 453 Yan Y.Y.: Land and Sea Breezes. In: Oliver J.E. (eds) *Encyclopedia of World Climatology*. Encyclopedia of Earth
454 Sciences Series. Springer, Dordrecht, 2005.
- 455
456



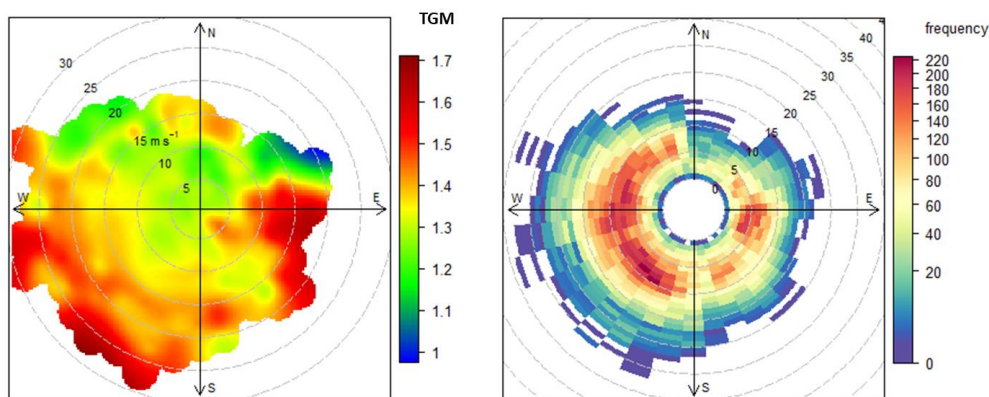
457
458
459
460

Figure 1. TGM hourly variations measured at Mace Head, from 2013 to 2018 (bottom), time series of mercury attributed to each factor (center) and time series of sea and combustion only (top).



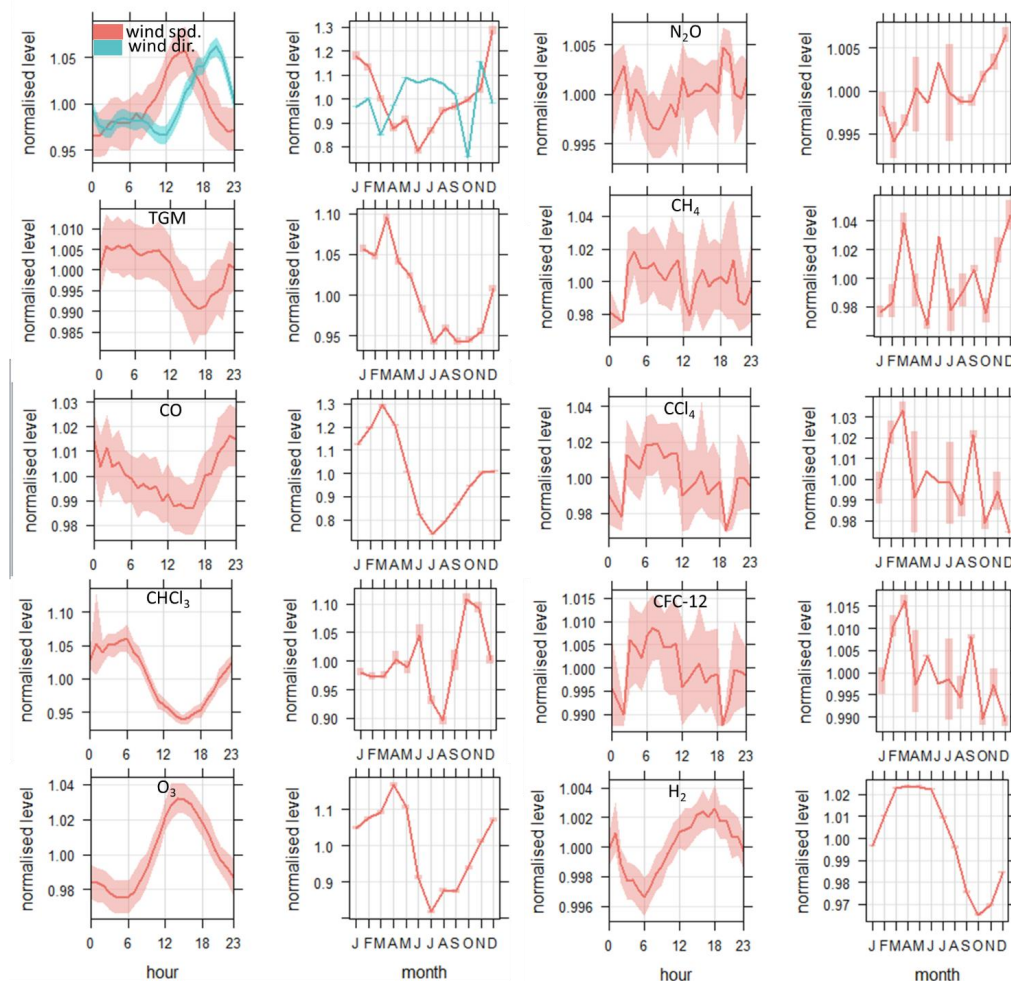
461
462
463

Figure 2. Time series decomposition of TGM (monthly averages) measured at Mace Head from 1996 to February 2018. * TGM in ng m^{-3} .



464
 465
 466

Figure 3. Polar plots for TGM (left) and polar wind frequency (right) at Mace Head. * TGM in ng m^{-3} and wind speed in ms^{-1} .



467
 468
 469

Figure 4: Diurnal cycle and seasonal cycle of mercury and species loaded in the PMF matrix. The shaded areas are the 95% confidence intervals in the mean. *Wind direction is normalised with 0° defined as North.



470
471
472
473
474
475
476
477
478
479
480
481
482
483
484
485
486
487
488
489
490
491
492
493
494

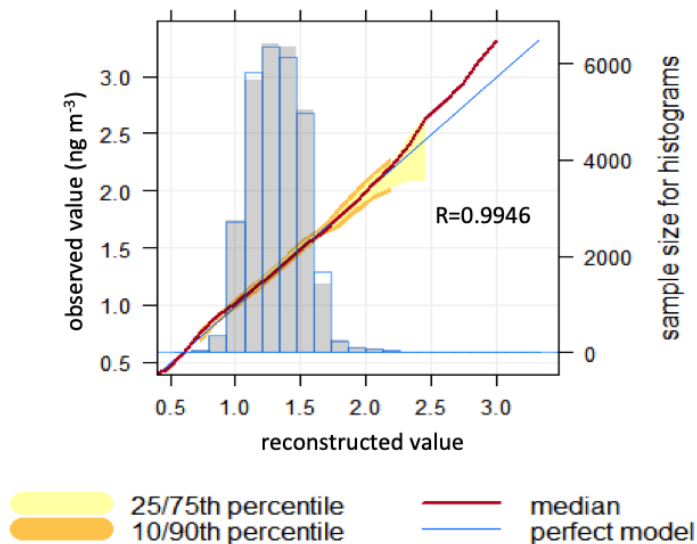


Figure 5: Correlation among total elemental mercury measured and mercury reconstructed by the PMF solution.

495
496
497
498
499
500
501

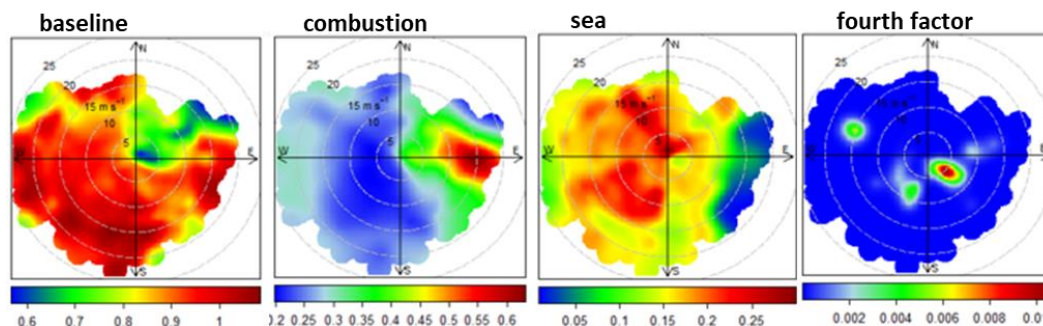
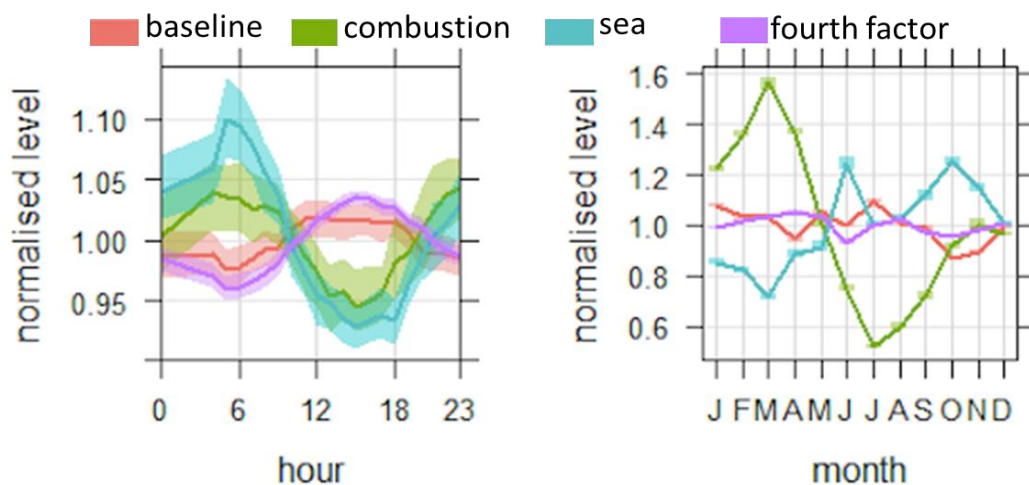
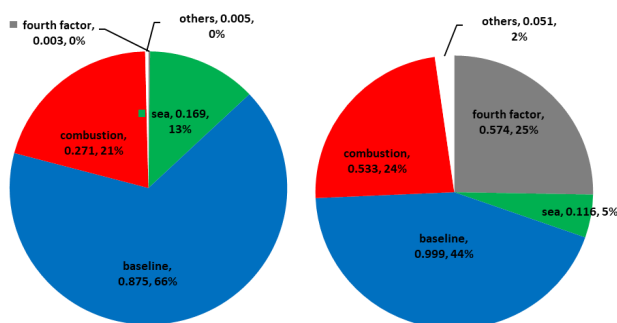


Figure 6. Polar plots for the factors obtained in the PMF solution. The plots show variations of mercury (ng m^{-3}) loaded in each factor as a function of wind direction ($^{\circ}$) and speed (ms^{-1}).



502
 503
 504
 505
 506
 507
 508
 509
 510
 511

Figure 7: Mean and 95% confidence interval in mean of diurnal and seasonal cycle of four PMF factors.



512
 513
 514
 515
 516
 517
 518

Figure 8. Average contribution (ng m⁻³ and %) of Hg⁰ factors for Mace Head from 2013 to 2018 (left) and mass closure for mercury concentration greater than 2 ng m⁻³ (right).